

Silicate Emission in T Tauri Stars: Evidence for Disk Atmospheres? ¹

Antonella Natta

Osservatorio Astrofisico di Arcetri, Largo Enrico Fermi 5, I-50125 Firenze, Italy

Michael R. Meyer²

Steward Observatory, The University of Arizona, 933 N. Cherry Ave.,
Tucson, AZ 85721-0065

and

Steven V.W. Beckwith³

Space Telescope Science Institute, 3700 San Martin Drive, Baltimore, MD 21218

ABSTRACT

We present low-resolution mid-infrared spectra of nine classical T Tauri stars associated with the Chamaeleon I dark cloud. The data were obtained with the PHOT-S instrument on-board the Infrared Space Observatory (ISO) in the two wavelength ranges 2.5–4.9 and 5.9–11.7 μm . All nine stars show evidence of silicate emission at 10 μm , which is the only prominent feature in the spectra. We discuss a model for the origin of these features in a hot optically-thin surface layer of the circumstellar disks surrounding the central young stars (i.e. a disk atmosphere). We report excellent agreement of our observations with predictions based upon this simple model for most stars in our sample, assuming that a mixture of amorphous silicates of radius $\lesssim 1 \mu\text{m}$ is the dominant source of opacity. These observations support the notion that extended disk atmospheres contribute substantially to the mid-IR flux of young stars.

Subject headings: circumstellar matter: disks — dust: silicate – stars: pre-main sequence – infrared: spectra

¹ Based on observations obtained with ISO. ISO is an ESA project with instruments funded by ESA Member States (especially the PI countries: France, Germany, the Netherlands and the United Kingdom) and with the participation of ISAS and NASA.

²Hubble Fellow

³also at the Max-Planck-Institut für Astronomie, Königstuhl 17, Heidelberg, Germany, D-69117

1. INTRODUCTION

It is generally recognized that circumstellar disks provide the most economical means of accounting for the spectral energy distributions of T Tauri stars. The extended, flat distributions of gas and dust can easily generate the observed broad spectral energy distributions (Lynden-Bell & Pringle 1974; Adams, Lada, & Shu 1987), and calculations of disk spectra have been successful at reproducing many observations of these stars (Calvet et al. 1992; D’Alessio et al. 1999; Chiang & Goldreich 1997, 1999). In some cases, the disks are apparent in images of the stars, either via scattered light or in silhouette against a background light source (Burrows et al. 1996; McCaughrean & O’Dell 1996).

The disks may be heated either radiatively by the central star or by energy released as matter accretes through the disk driven by turbulent viscosity. It is still a matter of debate which of these is more important for any given star, and the variety of spectral energy distributions observed indicates that the principal heating source may be different in various star+disk systems. It is important to determine the extent to which radiation or accretion dominates, because almost all other aspects of our understanding of these disks depends on the energy budget as a function of radius. For example, the amount of convection will depend on the vertical temperature gradient in the disk atmosphere.

A clear distinction between an atmosphere heated from the top by radiation and from the bottom by accretion is the presence of spectral features. An atmosphere heated from above by radiation will generally produce emission features, unless the viewing angle is very close to the plane of the disk. A disk heated from the mid-plane by accretion will have an atmosphere with a vertically decreasing temperature, and all spectral features will be in absorption. Observations of disk spectra should provide a good discriminant between these two possibilities. For example, FU Ori objects, a class of eruptive variables whose luminosities are dominated by accretion, exhibit deep absorption features due to their low surface gravity disk atmospheres (Kenyon & Hartmann, 1997).

Cohen & Witteborn (1985) showed that some T Tauri stars had broad resonance features near $10\ \mu\text{m}$, although it was not known at the time where these lines were formed and the signal-to-noise ratios were not high. We set out to verify if these emission features are the rule by observing a set of T Tauri stars with the spectrometer of ISOPHOT, PHOT-S, on the Infrared Space Observatory. In section II, we describe the observations and analysis of the data, while in section III we review the results. In section IV, we discuss the nature of the observed silicate feature with emphasis on comparison to predictions of the disk atmosphere model. Finally, in section V we summarize our results.

2. OBSERVATIONS AND DATA REDUCTION

We have selected a sample of nine well-studied TTS in the Chamaeleon I dark cloud. These objects are listed in Table 1 along with relevant stellar parameters taken or derived from the published literature. All the stars in this sample have an infrared excess, indicating the presence of a circumstellar disk or envelope. Source positions were taken from Gauvin & Strom (1992) and checked with Lopez & Girard (1990). Discrepancies in position were $< 10''$ for all sources.

We obtained spectrophotometric data of our sample during orbits 166 and 270 (on May 1 and August 14, 1996 respectively). We utilized the PHOT-S module of the ISOPHOT instrument (Lemke et al., 1996) providing a resolving power of $R \sim 50$ from 2.5–4.9 μm and 5.9–11.7 μm . The observations were performed in triangular-chop mode within approved observing template PHT40. Sky-positions were selected $90''$ north and south of the targets and the input aperture was $28'' \times 28''$. On-source integration times were 512 seconds per source. Dark current observations were obtained in order to monitor detector history effects.

The data were reduced using the Phot-Interactive Analysis (PIA) Version 7.3.2 (Gabriel et al. 1997)⁴. We utilized the two-threshold deglitching algorithm for the edited raw data and split each signal ramp into three sub-ramps. Slopes (in units of volts per second) were fit to each sub-division with a linear least-squares method. The distribution of slopes for each measurement was checked again and spikes were discarded. Dark subtraction was performed appropriate for the orbital time of the observations. The selected raw data were then averaged without attempting to correct for the drift behavior of the detector responsivity. Background signals were subtracted by interpolating between the two off-source chopper positions. The signal levels were then calibrated using a flux-dependent grating response function derived without drift-corrections. The resulting spectra for the nine stars observed are shown in Fig. 1 – 3 plotted in units of flux density (Jy). This calibration of the PHOT-S data available within PIA Version 7.3.2 should be accurate to $< 30\%$ in a relative sense and $< 30\%$ absolute (Klaas et al., 1998). The error bars in Fig. 1–3 reflect the random errors in signal derivation and not the systematic errors in calibration.

In order to verify our results, we reduced observations of two standard stars of different brightness; the M0 III star HR 6464 [$F_\nu(10\mu\text{m}) \sim 10.0$ Jy] and the K1 V star HD 132142 [$F_\nu(10\mu\text{m}) \sim 0.1$ Jy]. The data were processed identically to those of our program stars

⁴PIA is a joint development by the ESA Astrophysics Division and the ISOPHOT Consortium led by the Max-Planck-Institute for Astronomy (MPIA), Heidelberg.

and results were compared to the model atmosphere calculations described by Cohen et al. (1996). Comparison of the data to the predictions agreed within the errors of the models for the bright source ($< 3.3\%$ per pixel) and within the errors of the observations for the faint source ($< 25\%$ per pixel) over most of the $5.9\text{--}11.7\ \mu\text{m}$ spectral regime. In the bright standard, the model exhibits disagreement with the observed spectrum near $8.3\ \mu\text{m}$ where there is a hint of an unidentified feature at a maximum depth of 10% . In the $2.5\text{--}4.9\ \mu\text{m}$ band the bright source model disagrees systematically with the observations at $\lambda < 2.9\ \mu\text{m}$ and between $3.9\text{--}4.2\ \mu\text{m}$ ($< 5\%$) near the CO fundamental bandhead at $4.6\ \mu\text{m}$. In the faint standard, the data are systematically lower than the model between $3.0\text{--}3.6\ \mu\text{m}$ at the level of 10% . In general, these tests verify the applicability of our signal derivation algorithm and the internal consistency of the calibration procedure. However, features which appear at wavelengths where the models are clearly discrepant with the observations of the standard stars should be treated with suspicion. Details concerning the calibration of PHOT-S can be found in Acosta-Pulido et al. (2000).

3. RESULTS

3.1. The short-wavelength spectrum

The region between $2.5\text{--}4.9\ \mu\text{m}$ is featureless (within the noise) for most of the stars in our sample, with two possible exceptions. In WW Cha and VZ Cha there is some evidence of a broad absorption feature near $4\ \mu\text{m}$. Similar features have been observed in a survey of K giant stars by Decin & Vandebussche (private communication). Preliminary analysis suggests that they are instrumental artifacts though this has yet to be demonstrated conclusively. We do not see evidence for the $3.1\ \mu\text{m}$ H₂O nor the $4.3\ \mu\text{m}$ CO₂ ice-band features as seen in absorption toward heavily embedded young stellar objects (e.g. van Dishoeck et al. 1998).

3.2. The long-wavelength spectrum

The region between $5.9\text{--}11.7\ \mu\text{m}$ is characterized by the presence of the $10\ \mu\text{m}$ silicate feature, which is seen in emission in most of the stars in our sample. In addition, there is an underlying continuum emission, whose strength (relative to the silicate feature and the stellar photosphere) varies from star to star. We approximate this continuum as a power-law function of wavelength normalized in the spectral region $5.8\text{--}8\ \mu\text{m}$ (dashed lines in Fig. 1–3).

The shape of the feature varies somewhat from star to star. Three of the best measured spectra (Glass Ia, LkH α 332-20 and WW Cha) are quite similar, with a peak at about 10 μm and a slow rise on the blue side. The FWHM of these features after continuum subtraction is $\sim 2.8 \mu\text{m}$. Two other stars (CT Cha and SX Cha) have flatter spectra with no clear peak. We summarize the properties of the features in Table 2 which gives the name of the star, the luminosity of the feature between 7.5 and 11.6 μm after subtraction of the continuum component, the ratio of the luminosity in the feature to the stellar luminosity, and the ratio of the flux at the peak of the feature ($\sim 10 \mu\text{m}$) to the continuum at the same wavelength. The ratio L_{sil}/L_{\star} is 1–2 % for most stars, with the remarkable exception of Glass Ia where it is $\sim 10\%$ ⁵.

Gürtler et al. (1999) have also obtained spectra for two of the stars in our sample, Glass Ia and LkH α 332-20. Our observed flux for Glass Ia is intermediate between two observations taken at different epochs reported in Gürtler et al. (but closer to the one obtained nearest in time). The observed flux for LkH α 332-20 is similar to that reported by Gürtler et al. though the line shape is noticeably different. However, differences in line shape could be due to differences in reduction techniques ⁶. There is no evidence for emission from the unidentified infrared bands at 6.2 and 7.7 μm often attributed to polycyclic aromatic hydrocarbons (PAHs). Such features have been observed in the spectra of objects that illuminate reflection nebulosities (e.g. Gürtler et al., 1999). The 6.2 and 7.6 μm features lie in a region of the spectrum well measured in our data.

4. NATURE OF THE SILICATE EMISSION

The main interest of the silicate feature seen in these TTS spectra lies in the possibility it offers of investigating the optically thin dust component of the circumstellar environment. Historically, the feature has been described as optically thin emission from dust having optical depth τ_{ν} and temperature T_{BB} (Cohen and Witteborn 1985), with the possible addition of some line-of-sight extinction (Hanner et al. 1998). We prefer to follow a different approach, and compare the observed features to the predictions of specific models of the circumstellar environment of TTS. At present, the most interesting suggestion on the origin of the silicate emission is that of Calvet et al. (1992) and Chiang & Goldreich (1997; CG97), who point out that the feature could form in the optically thin surface

⁵However Glass Ia has an embedded companion of unknown luminosity that may excite the silicate emission as discussed in section 4.3 below

⁶We employed a more recent version of the PIA with an updated grating response function calibration.

layers of a circumstellar disk, heated well above the temperature of the disk midplane by the stellar radiation. An alternative possibility has been suggested for the binary star GW Ori, namely that the silicate emission originates in a disk “gap”, cleared by the dynamical perturbation of a companion star. A small amount of residual dust in the gap is heated by the stellar radiation to temperatures of few hundred degrees and causes the observed emission (Mathieu et al. 1991). This model predicts very little continuum emission in the 10 μm region, as observed in GW Ori, where there is clear evidence of a mid-infrared dip in the SED. This does not seem to be the case of the TTS in our sample (Robberto et al. 1999), and we will not discuss it further.

4.1. Model Calculations

We will follow here the very elegant and simple treatment of CG97 to predict the 10 μm feature intensity of each individual star, and we refer the reader to their paper for a more detailed description of the model. In CG97 models, the stellar radiation penetrates the disk outer layers to an optical depth $\tau^{\parallel} \sim 1$ along the disk plane. τ^{\parallel} is measured at the wavelength where the stellar flux F_{ν} peaks (roughly at frequency $\nu_{\star} \sim 2.1\text{-}3 \times 10^{14}$ hz (1–1.4 μm) for the stars in our sample). In the direction orthogonal to the disk surface, the optical depth at ν_{\star} is :

$$\tau^{\perp} = \tau^{\parallel} \alpha \sim \alpha \quad (1)$$

where α is the grazing angle. If the disk is in hydrostatic equilibrium in the vertical direction, α can be written as ($R \gg R_{\star}$):

$$\alpha \sim \frac{8}{7} \left(\frac{T_{\star}}{T_c}\right)^{4/7} \left(\frac{R}{R_{\star}}\right)^{2/7} \quad (2)$$

where R is the distance from the star and T_c measures the gravitational potential at the stellar surface:

$$T_c = \frac{GM_{\star} \mu}{KR_{\star}}. \quad (3)$$

K is the Stefan–Boltzman constant and μ is the mean molecular weight. This superheated layer is optically thin in the orthogonal direction at all wavelengths. Its emission can be easily computed as:

$$F_{\nu}^a = \frac{1}{D^2} \int_{R_{in}}^{R_{out}} 2\pi R dR B_{\nu}(T) \tau_{\nu}^{\perp} \quad (4)$$

$$F_{\nu}^a = \frac{8}{7} \frac{2\pi R_{\star}^2}{D^2} \left(\frac{T_{\star}}{T_c}\right)^{4/7} \left(\frac{\sigma_{\nu}}{\sigma_{\star}}\right) \int_{R_{in}/R_{\star}}^{R_{out}/R_{\star}} B_{\nu}(T) x^{9/7} dx \quad (5)$$

where D is the distance of the star, B_ν the Planck function, R_{in} and R_{out} the inner and outer radius of the dusty disk and $\tau_\nu^\perp = \alpha \times \frac{\sigma_\nu}{\sigma_\star}$, with σ_ν being the dust absorption cross section at ν and σ_\star being the dust cross section at ν_\star . The dependence of F_ν on the disk viewing angle is weak unless the disk is seen practically edge-on and occults the emission coming from the inner region of the disk itself (Chiang and Goldreich 1999).

The dust temperature T of grains in the optically thin atmosphere depends on the stellar radiation field and on the grain emissivity. For the cases we are considering, we have checked using the radiation transfer code kindly provided to us by E. Krügel that it can be expressed as a power-law function of the distance from the star R :

$$T \sim T_0 \left(\frac{R}{R_\star} \right)^{-q}. \quad (6)$$

with $q \sim 0.47$, $T_0 \sim 0.75T_\star$. For the stars in our sample, R_{in} , the distance from the star where the grains sublimate ($T \sim 1500$ K), varies between ~ 4 and $\sim 7R_\star$, depending on the stellar temperature. We have adopted $R_{out} = 100$ AU; the results are not sensitive to the exact value of these radii.

For each star, we have adopted the values of L_\star , R_\star , T_\star and M_\star given in Table 1. Once the stellar parameters are fixed, F_ν^a depends only on the dust cross section. To clarify the following discussion, we re-write the ratio σ_ν/σ_\star as the product $(\sigma_\nu/\sigma_{10}) \cdot (\sigma_{10}/\sigma_\star)$, where σ_{10} is the opacity at the peak of the silicate feature. The first term σ_ν/σ_{10} determines the shape of the feature and depends only on the specific properties of the silicates that dominate the feature (size, mineralogy, and allotropic form). The second term σ_{10}/σ_\star determines the feature intensity and is essentially the “efficiency” of converting stellar photons into silicate emission. This depends not only on the dust properties enumerated above, but also on attributes which determine the relative dust opacities from the visible/near-IR (σ_\star) to that near the feature itself in the mid-IR (σ_{10}); for example, the relative contribution of carbonaceous and silicate grains to σ_\star . After a preliminary exploration of a variety of silicates (see §4.2), we have adopted for σ_ν/σ_{10} the cross section of $1.2 \mu\text{m}$ radius pyroxene ($\text{Mg}(0.5)\text{Fe}(0.43)\text{Ca}(0.03)\text{Al}(0.04)\text{SiO}_3$; Jaeger et al. 1994) between 5.5 and $15 \mu\text{m}$, but kept as a free parameter $\epsilon = \sigma_{10}/\sigma_\star$. Note that ϵ is the only free parameter of these models.

The results are shown in Fig. 4. In each panel, the dots show the observed spectrum. The solid curve is the model prediction, computed by adding to the emission of the disk atmosphere the power-law continuum emission shown by the dashed lines in Fig. 1, 2, and 3. This characterization of the continuum emission is somewhat uncertain. CG97 compute the emission of the optically thick disk midplane in addition to that of the outer optically thin layers. One could, in principle, use their model to obtain values of the continuum emission consistent with the structure of the disk atmosphere required to reproduce the observed

silicate emission. However, contrary to the atmospheric emission in the 10 μm region, the contribution of the disk midplane to the continuum depends on the inclination of the disk with respect to the line of sight. Moreover, at wavelengths $\lambda < 10 \mu\text{m}$ the disk midplane emission is more sensitive to viscous heating and the inner disk radius (e.g. Meyer, Calvet, & Hillenbrand, 1997). Therefore, we defer the discussion of the continuum emission (and of its consistency with the results discussed in this paper) to a forthcoming contribution (Robberto et al. 2000) where we will make use of the broad-band fluxes measured by ISO over the wavelength range 3.4 – 200 μm (see Robberto et al. 1999 for a presentation of some preliminary results).

The value of $\epsilon = \sigma_{10}/\sigma_*$ which provides the best approximate fit to the observations given the assumptions outlined above is given in each panel. Note that for each star the model-predicted intensity of the feature (continuum subtracted) is simply proportional to ϵ .

4.2. Mineralogy

The assumption of the cross-section of 1.2 μm pyroxene grains for σ_ν/s_{10} in the model calculations gives a reasonable fit to the observed feature shapes. However, it is by no means unique. In our exploration of the effects of dust mineralogy on the shape of the feature, we have used as a reference the Glass Ia spectrum, because of its high signal-to-noise; the results would not be different for the other stars.

The model predictions for Glass Ia and a variety of amorphous silicates are shown in Fig. 5. We show results for olivine of radius 0.1 and 1 μm (MgFeSiO_4 ; Dorschner et al. 1995); for pyroxene grains of radius 0.1 and 1.2 μm ($(\text{Mg}(0.5)\text{Fe}(0.43)\text{Ca}(0.03)\text{Al}(0.04)\text{SiO}_3$; Jaeger et al. 1994), and for mixtures of olivine and pyroxene of 1 μm and 0.1 μm radius. Olivine or small pyroxene grains cannot reproduce the feature shape; a good fit is provided by rather large ($\sim 1 \mu\text{m}$) pyroxene grains and by mixtures of olivine and pyroxene of radii $\lesssim 1 \mu\text{m}$. Much larger grains can be excluded, since they give an emission feature peaked at too long wavelengths. The top panel of Fig. 5 shows the Glass Ia model predictions for Draine and Lee (1984; DL) astronomical silicates. The optical constants of such silicates were constrained to reproduce the shape of the 10 μm feature observed by Forrest et al. (1979) in the direction of the Trapezium stars for a MRN size distribution of grains, i.e., for the case when the opacity is dominated by small grains (Mathis et al., 1977). We find good agreement between the observations in the direction of Glass Ia and DL astronomical silicates; the only significant discrepancy occurs at long wavelengths, where the DL feature is broader. The Trapezium feature is significantly broader than that observed in the diffuse ISM (see Draine, 1989). The comparison with TTS seems to indicate that silicates in the

Trapezium region are similar to those in TTS disks, and are consistent with a mixture of amorphous olivines and pyroxenes.

Before discussing further our observations in the context of CG97 models, let us point out that we may have some evidence of two additional emission components at $8.5 \mu\text{m}$ and $11.3 \mu\text{m}$. Excess emission at long wavelengths with respect to model predictions is seen in almost all stars. A feature at $11.3 \mu\text{m}$ is typical of crystalline silicates, and it has been detected in SWS spectra of some pre-main-sequence stars of intermediate mass (Malfait et al. 1999a,b). However, our observational errors are larger at longer wavelengths, and the only clear case where we see a secondary peak at $\lambda \gtrsim 10 \mu\text{m}$ is Glass Ia. Also, the long-wavelength excess can be an artifact of our crude fitting of the continuum between $5.8\text{--}8 \mu\text{m}$. This can be checked by combining our PHOT-S data with observations at longer wavelengths. The spectrum of Glass Ia also shows that a second feature may be present with peak at about $8.5 \mu\text{m}$. This feature is seen in SWS spectra of some OH/IR and B[e] stars (Waters, personal communication). A possible attribution to SiO_2 is being investigated. However, this feature sits near the $8.3 \mu\text{m}$ region noted above for which the calibration is somewhat uncertain and so should be treated with caution. The absence of features at 6.2 and $7.6 \mu\text{m}$ rules out the possibility that the excess emission at ~ 8.5 and $11.3 \mu\text{m}$ could be due to PAHs.

4.3. Discussion

The CG97 models are remarkably successful in accounting for the observed emission. For 6 stars, ϵ is in the range 1–2.5. We cannot determine if the spread of values from star to star within this interval reflects different grain properties or uncertainties on the stellar parameters and inclination. However, we can compare the values derived from our model with those expected based on absorption cross-sections calculated for various types of grains. Amorphous olivine has $\epsilon \sim 1$ over a large range of sizes, while pyroxene grains generally require larger values of ϵ (~ 10 for micron-size grains and ~ 25 or larger for smaller grains). The olivine-pyroxene mixtures that reproduce the observed feature shapes have $\epsilon \sim 1 - 2$. Predictions for conglomerates and/or large particles give values of ϵ in the range 1–1.5. Henning and Stognienko (1996), for example, give $\epsilon \sim 0.9 - 1.2$ for conglomerates made of pyroxene, iron, and olivine. Pollack et al. (1994) compact grains, which include a mixture of silicates, iron, organic materials and water ice, have $\epsilon \sim 1 - 1.4$ (see Henning and Stognienko 1996). In all these cases, the predicted shape of the feature should be similar to the observed one. It is also possible to reproduce the required ϵ value with pyroxene grains, if there is a contribution to the $1 \mu\text{m}$ opacity from carbonaceous

grains. However this contribution must be significantly smaller than in the interstellar medium; the MRN model of interstellar extinction of Draine and Lee (1984) has a $1 \mu\text{m}$ opacity dominated by graphite and $\epsilon \sim 0.2 - 0.3$, depending on the exact value of T_\star . In summary, amorphous olivine and pyroxene mixtures can roughly reproduce both the intensity and the shape of the observed features for most of the TTS in our sample. Large pure pyroxene grains cannot be excluded, as long as some additional opacity at visual and near-infrared wavelengths is provided by grains other than silicates.

In two cases we find much higher values of ϵ , i.e., silicate emission much stronger than predicted by the CG97 models with $\epsilon \sim 1 - 2.5$. One (XX Cha) is a very faint object and has a poorly measured spectrum, but the other (Glass Ia) is the strongest and best measured object in our sample. Glass Ia has the exceptionally large ratio $L_{\text{sil}}/L_\star \sim 10\%$, which requires for the stellar parameters given in Table 1 $\epsilon \sim 13$. Pyroxene grains of radius $1\text{--}1.2 \mu\text{m}$ (which fit well the shape of the feature) have $\epsilon \sim 10$. It is tempting to speculate that very strong silicate features may occur when the dust opacity is dominated by pyroxene grains over the whole range of wavelengths $\sim 1 - 10 \mu\text{m}$. However, we should point out that Glass Ia is a rather complex object. It is a binary system, with an infrared companion (IRC; component b) at a separation of about $2.7''$ (Chelli et al. 1988). Feigelson and Kriss (1989) report that this faint companion is an emission-line star of intermediate spectral type (G3–G7). Although component b is very faint in the visible, it dominates the emission at wavelengths longer than $2.0 \mu\text{m}$ (Chelli et al. 1988). There are a handful of such objects known in T Tauri systems, where the IRC is responsible for the bulk of the IR emission and is thought to be in an earlier evolutionary state. Recent, unpublished $10 \mu\text{m}$ wide-band images (Robberto et al. and Stanke and Zinnecker, private communications) confirm that the $10 \mu\text{m}$ emission comes from a single source, very likely Glass Ib. We have computed the silicate emission of Glass Ib, assuming a *stellar* luminosity (neglecting the contribution of active accretion) of $3.2 L_\odot$, an effective temperature of 5400 K and a mass of $2 M_\odot$ (e.g. Koresko et al. 1997); the value of ϵ we derive is ~ 12 , similar to that obtained under the assumption that Glass Ia is powering the feature.

A comparison of silicate spectra obtained for Glass Ia with observations of other T Tauri+IRC systems sheds no light on the matter. Spatially unresolved observations of T Tauri N & S indicate a nearly featureless $10 \mu\text{m}$ continuum (Hanner et al. 1998). However, spatially resolved $10 \mu\text{m}$ observations show that silicate emission is associated with the visible star, while the IR companion has silicate in absorption (Herbst et al. 1997). SX Cha, the other star in our sample with an IRC, has a rather normal silicate emission feature. It is possible that in Glass Ia the silicate emission forms not in a disk, but in a more spherically distributed warm dust component. We cannot solve this puzzle with the data presently available. Any model which adequately explains the silicate emission feature in

this system, must also explain its variability (cf. Gürtler et al. 1999). For the moment, the best explanation is that in Glass Ia or in Glass Ib the dust has an anomalous composition, perhaps including a small contribution from crystalline silicates.

Only one star in our sample (VW Cha) has a very small ratio L_{sil}/L_{\star} and a low value of ϵ (and a rather noisy spectrum). There are a number of effects that, in principle, can result in a silicate feature somewhat weaker than predicted by CG97 models. Firstly, the disk flaring may be smaller than assumed in CG97. This may happen, for example, if the dust is not well mixed with the gas, or if the temperature gradient in the vertical direction affects the density profile, which CG97 compute from the condition of hydrostatic equilibrium of an isothermal gas (see discussion in Kenyon and Hartmann 1987). Second, in cases where the disk is seen nearly edge-on, one does expect to observe silicate features in absorption as observed in a few cases by Cohen and Wittetborn (1985) and as modelled by Chiang and Goldreich (1999). A third important point is that heating of the disk by viscous dissipation of accretion energy may invert the vertical temperature gradient, so that the temperature is higher in the disk midplane than in the outer layer. In this extreme case, the feature should appear in absorption (Calvet et al. 1992). In reality, this is probably rarely the case, since about half of the accretion luminosity is emitted as UV radiation near the stellar surface and may contribute to the radiative heating of the disk outer layer (D’Alessio et al. 1998). In fact, FU Ori, where the accretion luminosity is much larger than the photospheric one, has very weak silicate emission (Hanner et al. 1998). A study of the SED of VW Cha over the whole range from UV to millimeter wavelengths, which can shed light on its properties, is deferred to a forthcoming paper (Robberto et al. 2000).

To summarize, the comparison with CG97 models provides a strong indication that; i) most TTS disks must be flared approximately as predicted by hydrostatic equilibrium models; ii) accretion, when present, does not dominate the disk heating, which is mostly due to stellar radiation at radii $\gg 0.1$ AU; and iii) the viewing geometry for the stars in our sample is not perfectly edge-on.

5. SUMMARY AND CONCLUSIONS

We have presented in this paper PHOT-S spectra of nine classical TTS in Chamaeleon. The spectra cover the wavelength ranges 2.5–4.9 and 5.9–11.7 μm . The only prominent feature in the spectra is the silicate emission feature at about 10 μm , which is seen in all the observed stars.

We discuss the possibility that the feature forms in the outer, optically thin layers of a circumstellar disk. If the disk heating is dominated by the stellar radiation, this disk atmosphere is hotter than the disk midplane, and emission features may be seen. We have followed the description of the disk atmosphere developed by Chiang and Goldreich (1997), and computed the predicted silicate feature for each star in our sample. We find good agreement between the model predictions and the observations for most stars.

In these models, the shape of the feature depends on the properties (size, chemical composition and allotropic form) of the silicates that dominate the $10\ \mu\text{m}$ opacity, while its intensity depends on the ratio (ϵ) of the opacity at the peak of the feature to the opacity at the wavelength where the stellar radiation is maximum. These are the only free parameters of the models, once the stellar properties (luminosity, effective temperature and mass) are known. For six stars out of nine a good fit between models and observations is obtained with values of $\epsilon \sim 1 - 2.5$, much larger than in the diffuse ISM, where $\epsilon \sim 0.2 - 0.4$. This, and the analysis of the shape of the features, suggests that silicates in the TTS disks are likely to be a mixture of amorphous olivine and pyroxene grains with radii $\lesssim 1\ \mu\text{m}$, with little contribution to the visual and near-infrared opacity from other dust components. Alternatively, our observations can be reproduced by large ($\sim 1\ \mu\text{m}$) pyroxene grains, with a significant contribution to the short-wavelength opacity from grains other than silicates.

The identification of disk atmospheres as the origin of silicate emission is certainly not a unique explanation. Full disk models, capable of reproducing both the silicate spectrum and the observed continuum over a large range of wavelengths need to be computed. Disk parameters, such as inclination, accretion luminosity, etc., have to be consistent with what we know about each individual star. Broad-band PHOT observations of the same TTS discussed here over the wavelength range $3.4\text{--}200\ \mu\text{m}$ have been obtained and are currently being investigated (Robberto et al. 2000). However, the results presented here give already some interesting information on the disk properties. As discussed in §4, we have assumed that the disk is in hydrostatic equilibrium in the vertical direction (flared). Atmospheres of flat disks are much less extended, and will reproduce the observed silicate emission only for unreasonably large values of ϵ ($\gtrsim 100$). Secondly, strong heating due to accretion in the disk midplane will reduce or suppress the inverse temperature gradient in the vertical direction and reduce the strength of the silicate emission. In the stars we observed, accretion is likely to contribute only marginally to the disk heating at radii $> 0.1\ \text{AU}$.

We gratefully acknowledge Bruce Draine, Thomas Henning, Malcolm Walmsley, and Endrik Krügel for helpful discussions, the referee for a helpful and informative review of this work, and Greet Decin, Bart Vandenbussche, Jörgen Gürtler, and Rens Waters for sharing information regarding PHOT-S data. Special thanks to Jose Acosta-Pulida as well as Peter

Abraham for assistance with the data reduction and calibration procedures. This work was partly supported by ASI grant ARS-98-116 to the Osservatorio di Arcetri. Support for MRM was provided by NASA through Hubble Fellowship Grant # HF-01098.01-97A awarded by the Space Telescope Science Institute, which is operated by the Association of Universities for Research in Astronomy, Inc., for NASA under contract NAS 5-26555.

REFERENCES

- Adams, F.C., Lada, C.J., & Shu, F.H. 1987, *ApJ*, 312, 788.
- Acosta-Pulida et al. 2000, *A&A*, in preparation.
- Beckwith, S.V.W., Henning, Th., & Nakagawa, Y. 2000, *Protostars and Planets IV*, eds. V. Mannings, A.P. Boss and S.R. Russell (Tucson: U. of A. Press), in press.
- Burrows, C.J., Stapelfeldt, K.R., Watson, A.M., et al. 1996, *ApJ*, 473, 437.
- Calvet, N., Magris, G.C., Patino, A., & D’Alessio, P. 1992, *RMA&A*, 24, 27.
- Chelli, A., Cruz-Gonzalez, I., Zinnecker, H., Carrasco, L., & Perrier, C. 1988, *A&A*, 207, 46.
- Chiang, E.I., & Goldreich, P. 1997, *ApJ*, 490, 368.
- Chiang, E.I., & Goldreich, P. 1999, *ApJ*, 519, 279.
- Cohen, M., & Witteborn, F.C. 1985, *ApJ*, 294, 345.
- Cohen, M., et al. 1996, *AJ*, 112, 2274.
- D’Alessio, P., Calvet, N., Hartmann, L., Lizano, S., & Canto, J. 1999, *ApJ*, in press.
- D’Alessio, P., Cantó, J., Calvet, N., & Lizano, S. 1998, *ApJ*, 500, 427.
- D’Antona, F. & Mazzitelli, I. 1994, *ApJS*, 90, 467.
- Dorschner, J., Begemann, B., Henning, Th., Jaeger, C., & Mutschke, H. 1995, *A&A*, 300, 503.
- Draine, B.T. 1989, *ESA-SP 290*, 93.
- Draine, B.T., & Lee, H.M. 1984, *ApJ*, 285, 89.
- Feigelson, E.D., & Kriss, G.A. 1989, *ApJ*, 338, 262.
- Forrest, W.J., McCarthy, J.F., & Houck, J.R. 1979, *ApJ*, 233, 611.
- Gabriel, C. et al. 1997, *Astronomical Data Analysis Software and Systems VI*, eds. G. Hunt and H.E. Payne (San Francisco: ASP), 125, 108.
- Gauvin, L., & Strom, K.M. 1992, *ApJ*, 385, 217.

- Ghez, A. et al. 1997, *ApJ*, 481, 378.
- Gürtler, J., Schreyer, K., Henning, Th., Lemke, D., & Pfau, W. 1999, *A&A*, 346, 205.
- Hanner, M.S., Brooke, T.Y., & Tokunaga, A.T. 1998, *ApJ*, 502, 871.
- Hartmann, L., & Kenyon, S.J., *ARA&A*, 34, 207.
- Henning, Th., & Stognienko, R. 1996, *A&A*, 311, 291.
- Herbst et al. 1997, *AJ*, 114, 744.
- Jaeger, C., Mutschke, H., Begemann, B., Dorschner, J., & Henning, Th. 1994, *A&A*, 292, 641.
- Kenyon, S.J., & Hartmann, L. 1987, *ApJ*, 323, 714.
- Klaas, U., Lemke, D., Kranz, T., et al. 1998, *Proc. SPIE Vol.3354, Infrared Astronomical Instrumentation*, A.M. Fowler Ed., p.996.
- Koresko, C.D., Herbst, T.M., & Leinert, Ch. 1997, *ApJ*, 480, 741.
- Lemke, D., Klaas, U., Abolins, J., et al. 1996, *A&A*, 315, L64.
- Lopez, C.E., & Girard, T.M. 1990, *PASP*, 102, 1018.
- Lynden-Bell, D., & Pringle, J.E. 1974, *MNRAS*, 168, 603.
- Malfait, K., Waelkens, C., Bouwman, J., De Koter, A., & Waters, L.B.F.M 1999a, *A&A*, 345, 181.
- Malfait, K., Waelkens, C., Waters, L.B.F.M., Vandenbussche, B., Huygen, E., & De Graauw, M.S. 1999b, *A&A*, 332, L25.
- Mathieu, R.D., Adams, F.C., & Latham, D.W. 1991, *AJ*, 101, 2184.
- Mathis, J.S., Rumpl, W., & Nordsieck, K.H., 1977, *ApJ*, 217, 425 (MRN).
- McCaughrean, M.J., & O'Dell, C.R. 1996, *AJ*, 111, 1977.
- Meyer, M.R., Calvet, N., & Hillenbrand L.A. 1997, *AJ*, 114, 288.
- Meyer, M.R. 1996, PhD Thesis, The University of Massachusetts.
- Pollack, J.B., Hollenbach, D., Beckwith, S., Simonelli, D.P., Rush, T., & Fong, W. 1994, *ApJ*, 421, 615.
- Robberto, M., et al. 1999, *The Universe as Seen by ISO*, P. Cox and M.F. Kessler Eds., (Noordwijkerhout: ESA), p.195.
- Robberto, M., et al. 2000, in preparation.
- van Dishoeck, E. et al. 1998, *ApJ*, 502, L173.

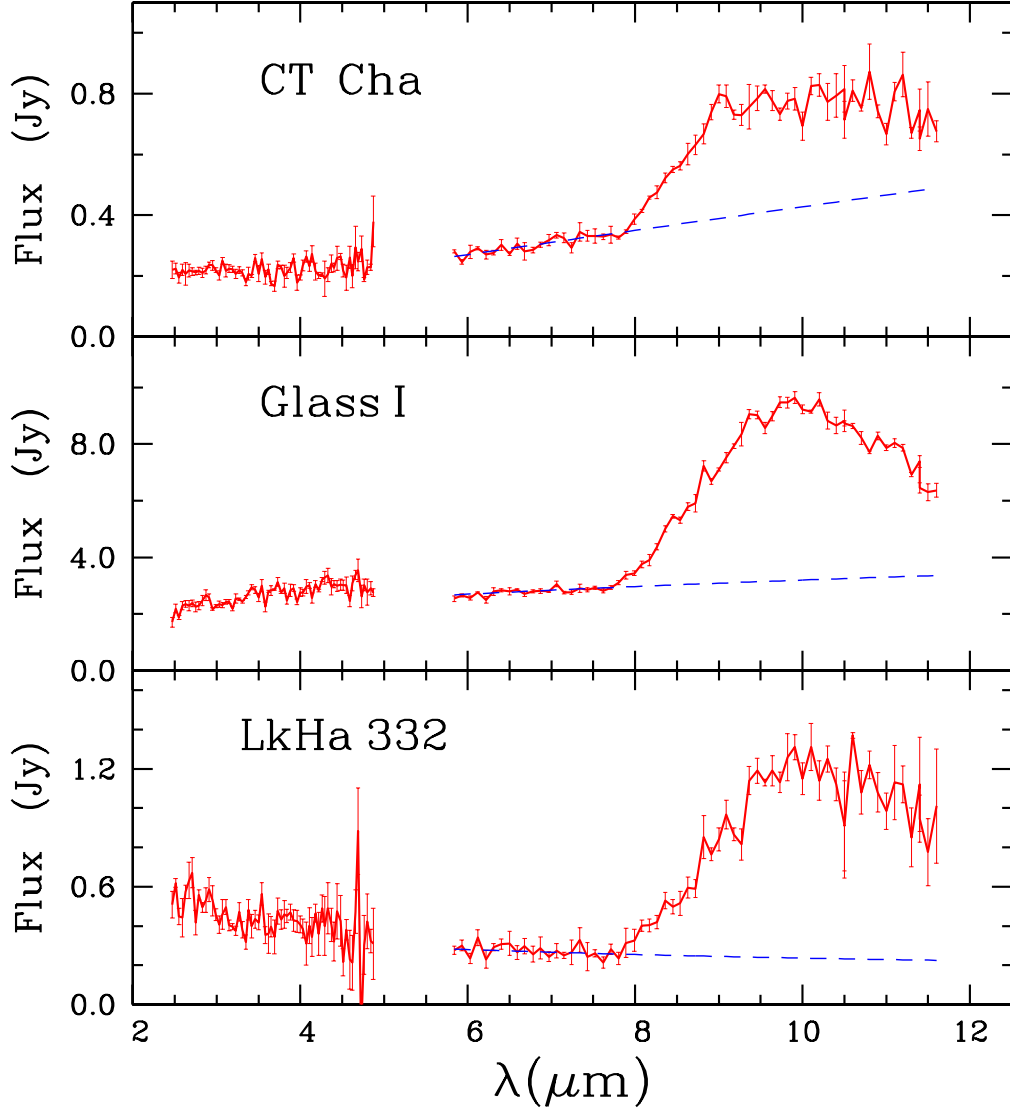


Fig. 1.— Observed spectra for CT Cha, Glass Ia, and LkH α 332-20. The dashed lines in Fig. 1–3 show for each star linear fits to the spectral region 5.8–8 μm .

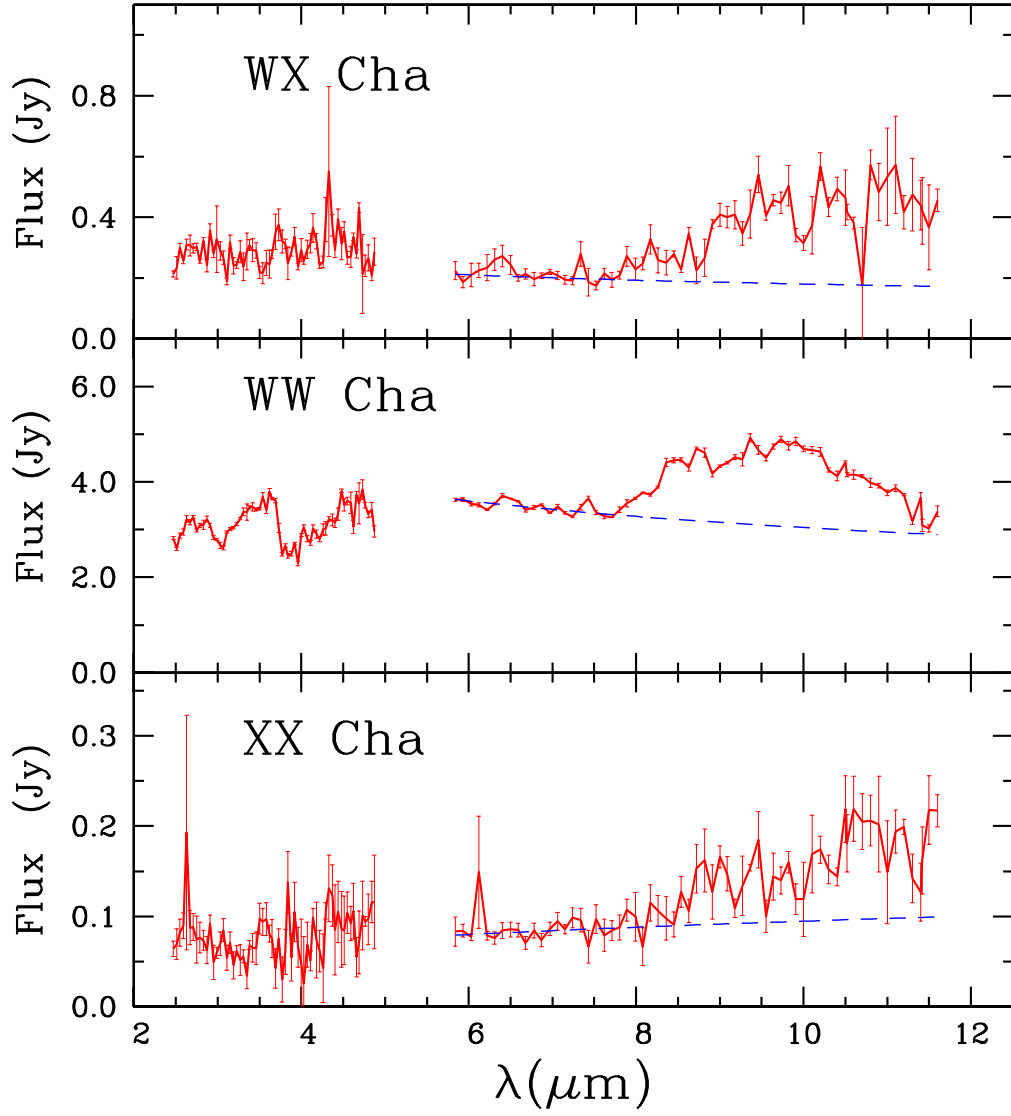


Fig. 2.— Same as Fig. 1 for SX Cha, VW Cha, and VZ Cha.

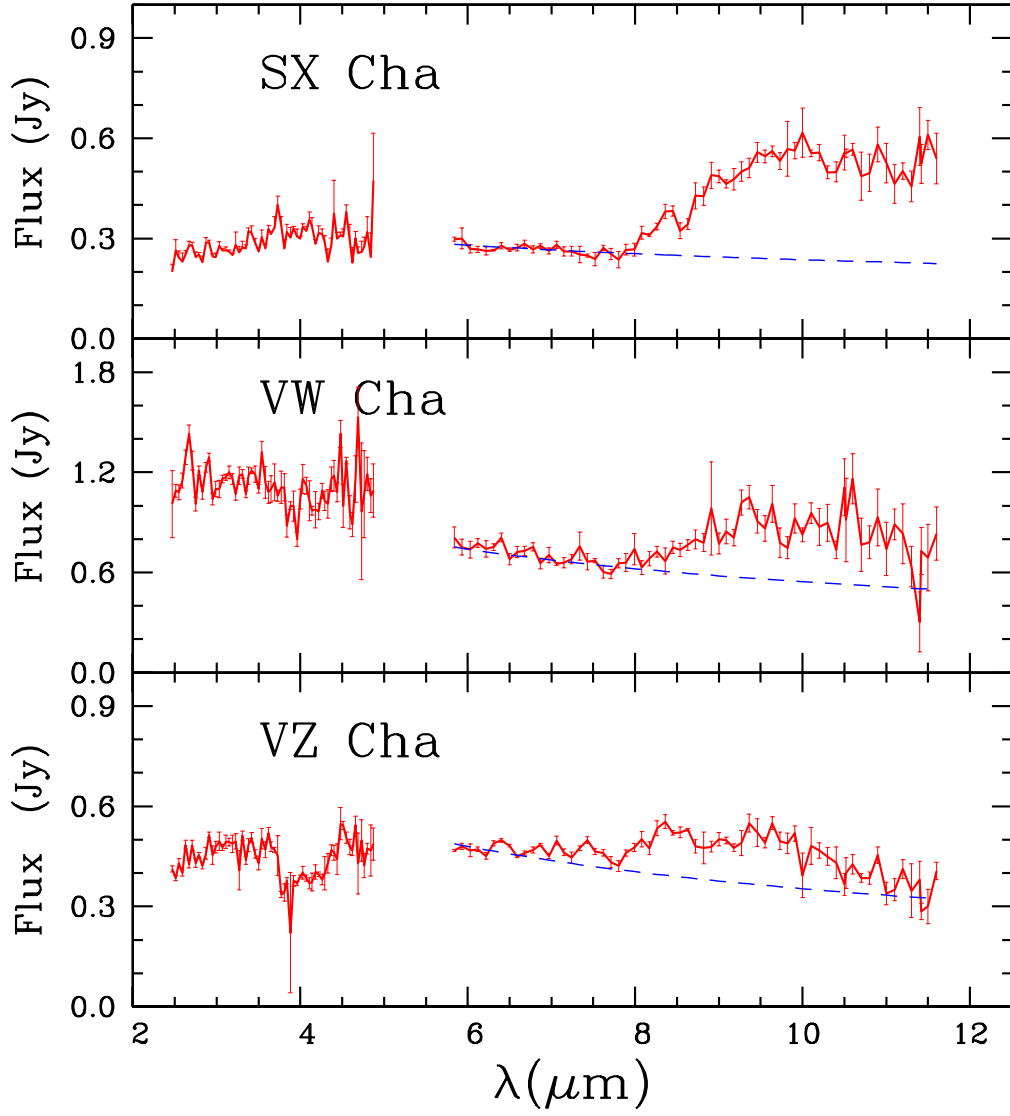


Fig. 3.— Same as Fig. 1 for WX Cha, WW Cha, and XX Cha.

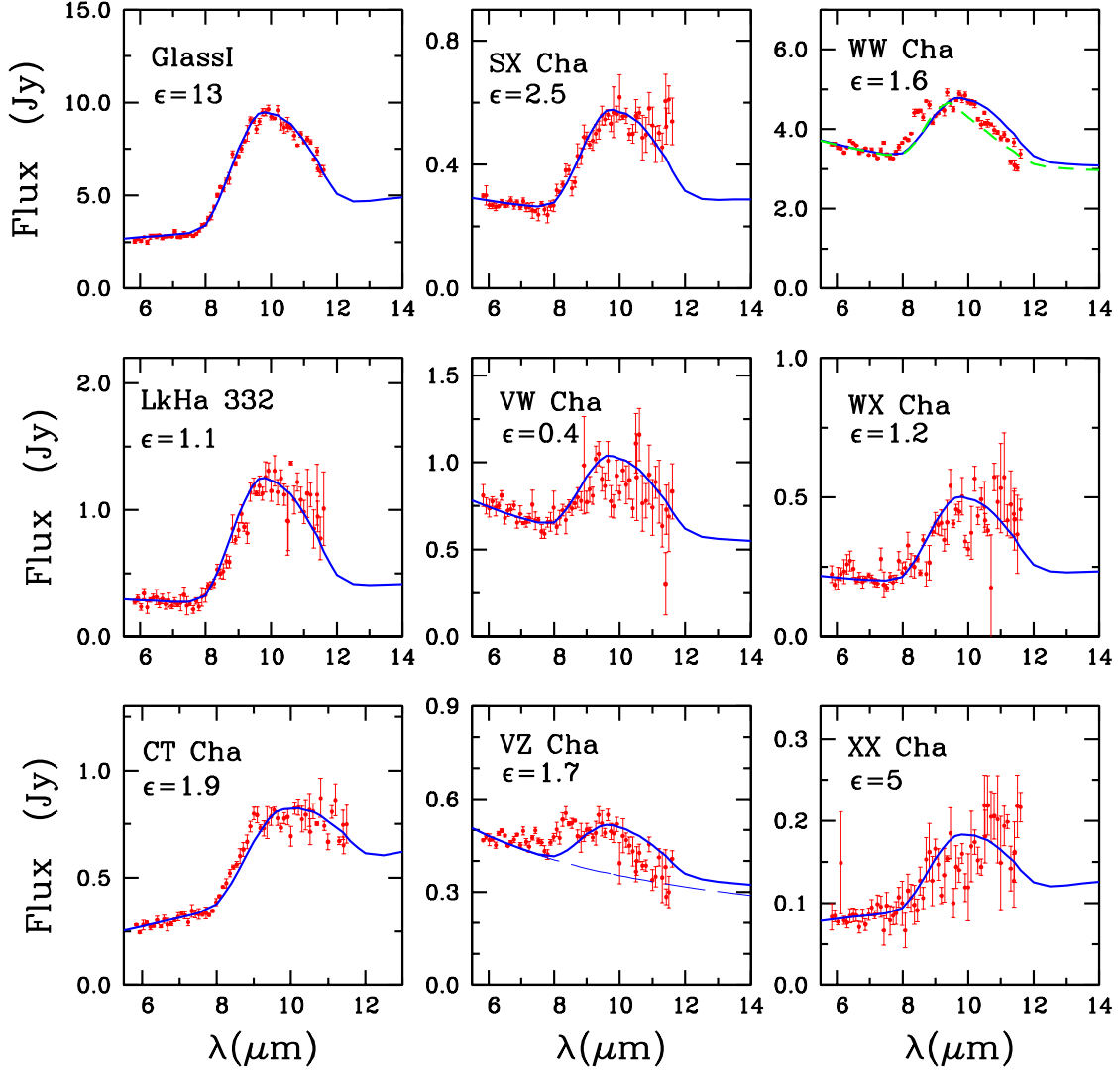


Fig. 4.— Model fits to the observed spectra. In each panel, the dots show the observed points. The solid line shows the predicted emission of the superheated disk atmosphere, computed following Chiang & Goldreich (1997) for pyroxene grains of $1.2 \mu\text{m}$ radius, overlaid on the continuum emission shown by the dashed lines in Fig. 1, 2, and 3. In the WW Cha panel, the dashed line shows the model predictions for small pyroxene grains ($0.1 \mu\text{m}$ radius); in the VZ Cha panel, the long-dashed line is the assumed continuum emission. The value of $\epsilon = \sigma_{10}/\sigma_*$ which gives the best approximate fit to the observations is given in each panel.

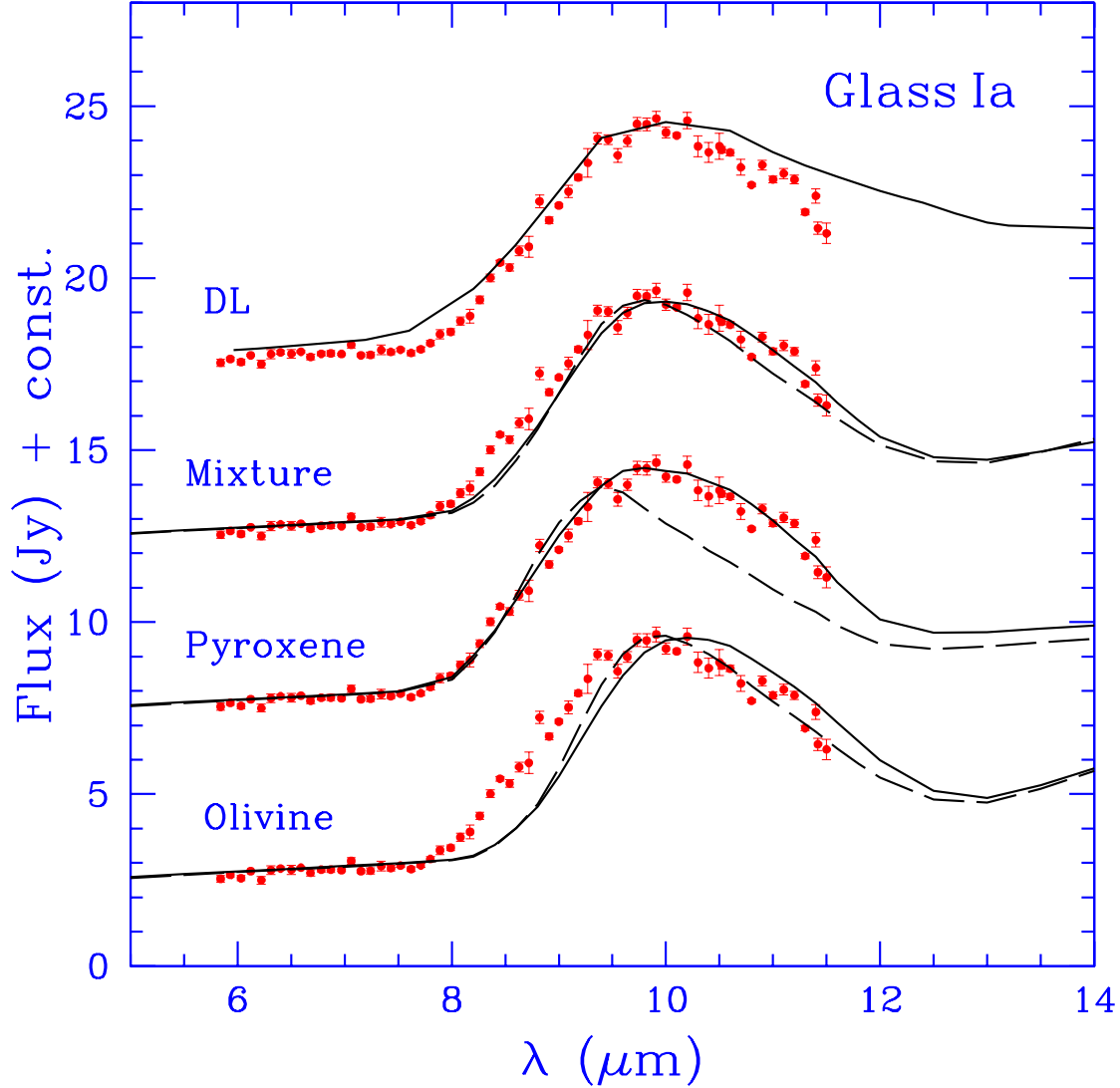


Fig. 5.— Model predictions for Glass Ia using different silicates. From top to bottom, we have: DL astronomical silicates; mixture of 0.5:0.5 olivine and pyroxene of $1 \mu\text{m}$ radius (solid line) and 0.3:0.7 of $0.1 \mu\text{m}$ radius (dashed line); pyroxene grains of radius $0.1 \mu\text{m}$ (dashed line), $1.2 \mu\text{m}$ (solid line); olivine grains of radius $0.1 \mu\text{m}$ (dashed line) and $1 \mu\text{m}$ (solid line). The model-predicted profiles have been scaled to reproduce roughly the observed peak intensity. The values of ϵ required to fit the feature are all in the interval 12–13.5. They can be compared to the values derived from the cross sections of these various minerals, which are 10 and 21 for pyroxene of 1.2 and $0.1 \mu\text{m}$ radius, 0.6 and 1.2 for 1 and $0.1 \mu\text{m}$ pyroxene, 2.2 for the 0.5:0.5 mixture of $1 \mu\text{m}$ grains, and 0.84 for the 0.3:0.7 mixture of $0.1 \mu\text{m}$ grains. The observations are shown by dots.

Table 1: Stellar Parameters

Name	SP ¹	T _★ (K)	EW(H α) ¹ (Å)	Compan. ²	L _★ ³ (L _☉)	R _★ ³ (R _☉)	M _★ ⁴ (M _☉)	Age ⁴ (Myr)
CT Cha	K7	4000	49.2	NC ^a	0.7	1.8	0.5	0.9
Glass Ia	K4	4600	4.0	2.8''/0.32 ^b	1.6	2.1	0.9	1.0
LkHα 332-20	K2	4900	43.6	NC ^a	3.3	2.6	1.2	1.0
SX Cha	M0.5	3700	26.7	2.1''/4.7 ^c	0.5	1.7	0.4	0.8
VW Cha	K5	4350	146.9	0.7''/4.5 ^a	2.9	3.1	0.6	0.3
VZ Cha	K6	4200	71.4	NC ^a	0.5	1.3	0.7	3.0
WX Cha	K7-M0	3900	65.5	0.8''/10 ^a	0.8	2.0	0.4	0.7
WW Cha	K5	4350	67.4	NC ^a	2.7	3.0	0.6	0.3
XX Cha	M1	3650	133.5	–	0.1	0.85	0.5	7.0

¹ Spectral information taken from Gauvin & Strom (1992).

² Presence or absence of companions ($d < 14''$) taken from a) Ghez et al. (1997); b) Chelli et al. (1988); or c) Robberto et al. (2000). For known doubles, the separation is given in arcseconds followed by the 2.2 μm flux ratio [F_{2.2} (optical primary)/F_{2.2}(IR companion)].

³ Stellar luminosity is calculated from bolometric corrections applied to dereddened I-band magnitudes following Meyer (1996) and the stellar radius is derived from the Stefan–Boltzman equation.

⁴ Masses and ages are derived from comparison of stellar effective temperatures and luminosities with the pre–main sequence evolutionary tracks of D’Antona & Mazzitelli (1994) using CM convection and Alexander opacities.

Table 2: Properties of the Silicate Feature

Name	L _{sil} (10 ⁻² L _☉)	L _{sil} /L _★ (%)	F _{peak} /F _{cont}
CT Cha	1	1.4	2.2
Glass Ia	17	10	2.6
LkHα 332-20	3	2	3.7
SX Cha	1	0.8	1.4
VW Cha	0.7	0.2	0.4
VZ Cha	0.2	0.5	0.2
WX Cha	0.8	1	1.7
WW Cha	5	1.8	0.5
XX Cha	0.2	2	1.2